Comparison of Physical and Photophysical Properties of Monometallic and Bimetallic Ruthenium(II) Complexes Containing Structurally Altered Diimine Ligands

Ariel Macatangay,[†] Greg Y. Zheng,[‡] D. Paul Rillema,*[,†,‡] Donald C. Jackman,[†] and Jon W. Merkert[†]

Departments of Chemistry, The University of North Carolina at Charlotte, Charlotte, North Carolina 28223, and Wichita State University, Wichita, Kansas 67260-0051

Received October 18, 1995[⊗]

The physical and photophysical properties of a series of monometallic, $[Ru(bpy)_2(dmb)]^{2+}$, $[Ru(bpy)_2(BPY)]^{2+}$, $[Ru(bpy)(Obpy)]^{2+}$ and $[Ru(bpy)_2(Obpy)]^{2+}$, and bimetallic, $[\{Ru(bpy)_2\}_2(BPY)]^{4+}$ and $[\{Ru(bpy)_2\}_2(Obpy)]^{4+}$, complexes are examined, where bpy is 2,2′-bipyridine, dmb is 4,4′-dimethyl-2,2′-bipyridine, BPY is 1,2-bis(4-methyl-2,2′-bipyridin-4′-yl)ethane, and Obpy is 1,2-bis(2,2′-bipyridin-6-yl)ethane. The complexes display metal-to-ligand charge transfer transitions in the 450 nm region, intraligand $\pi \rightarrow \pi^*$ transitions at energies greater than 300 nm, a reversible oxidation of the ruthenium(II) center in the 1.25−1.40 V vs SSCE region, a series of three reductions associated with each coordinated ligand commencing at −1.3 V and ending at ∼−1.9 V, and emission from a ^{3}MLCT state having energy maxima between 598 and 610 nm. The Ru^{III}/Ru^{II} oxidation of the two bimetallic complexes is a single, two one-electron process. Relative to $[Ru(bpy)_2(BPY)]^{2+}$, the Ru^{III}/Ru^{II} potential for $[Ru(bpy)_2(Obpy)]^{2+}$ increases from 1.24 to 1.35 V, the room temperature emission lifetime decreases from 740 to 3 ns, and the emission quantum yield decreases from 0.078 to 0.000 23. Similarly, relative to $[\{Ru(bpy)_2\}_2(BPY)]^{4+}$, the Ru^{III}/Ru^{II} potential for $[\{Ru(bpy)_2\}_2(Obpy)]^{4+}$ increases from 1.28 to 1.32 V, the room temperature emission lifetime decreases from 770 to 3 ns, and the room temperature emission quantum yield decreases from 0.079 to 0.000 26. Emission lifetimes measured in 4:1 ethanol:methanol were temperature dependent over 90−360 K. In the fluid environment, emission lifetimes display a biexponential energy dependence ranging from 100 to 241 cm^{-1} for the first energy of activation and 2300−4300 cm^{-1} for the second one. The smaller energy is attributed to changes in the local matrix of the chromophores and the larger energy of activation to population of a higher energy dd state. Explanations for the variations in physical properties are based on molecular mechanics calculations which reveal that the Ru−N bond distance increases from 2.05 Å (from Ru^{II} to bpy and BPY) to 2.08 Å (from Ru^{II} to Obpy) and that the metal-to-metal distance increases from ∼7.5 Å for $[\{Ru(bpy)_2\}_2(Obpy)]^{4+}$ to ∼14 Å for $[\{Ru(bpy)_2\}_2(BPY)]^{4+}$.

Introduction

The assembly of molecular components into an organized system for affecting energy transfer, electron transfer, and/or catalysis represents a synthetic challenge for chemists. Such assemblies fall in the nanotechnology area and have been called supramolecular complexes,[1,2] especially if they contain more than one metal center. Our own efforts have focused on developing such assemblies for solar energy photocatalysts. Our initial designs consisted of multimetallic complexes bridged by diimine ligands containing remote coordination sites.[3] In most cases, attachment of a second metal center to such a "piggyback" ligand lowered the energy of the π^* energy levels, resulting in very weak emission compared to the intensity of emission from the monometallic precursors. Thus, we have now turned our attention to bridging ligands where the diimine binding sites are separated by a molecular spacer. Intense emission has been observed from bimetallic complexes based on these types of bridging ligands[4] as well as intramolecular electron[5] and energy[6] transfer in heterobimetallic compounds.

The influence of the molecular spacer on molecular properties has been examined by others. Recently Meyer and co-workers[7] reported that complexes having an ethylene bridge between two bipyridine units exhibited long-lived, low energy luminescence. Prior to that, Schmehl and his research group examined the role of intraligand excited states associated with polyunsaturated bridging diimine ligands coordinated to ruthenium(II) and rhenium(I).[8] Until now, no one to our knowledge has directed their attention to alterations in photophysical properties of multimetallic complexes resulting from the site of molecular bridge attachment.

The ligands chosen to examine this issue are illustrated in Figure 1. As shown, the ligands are basically the same, except

* To whom correspondence should be addressed.
† The University of North Carolina at Charlotte.
‡ Wichita State University.
⊗ Abstract published in *Advance ACS Abstracts,* October 15, 1996.

(1) Balzani, V.; Scandola, F. *Supramolecular Photochemistry*; Horwood: Chichester, U.K., 1991.
(2) Schneider, H. J.; Duerr, H. *Frontiers in Supramolecular Organic Chemistry and Photochemistry*; VCH: Weinheim, Germany, 1991.
(3) (a) Rillema, D. P.; Callahan; R. W.; Mack; K. B. *Inorg. Chem.* **1982**, *21*, 2589. (b) Rillema, D. P.; Mack, K. B. *Inorg. Chem.* **1982**, *21*, 3849. (c) Sahai, R.; Rillema, D. P. *Inorg. Chim. Acta* **1986**, *188*, L32. (d) Sahai, R.; Rillema, D. P. *J. Chem. Soc., Chem. Commun*. **1986**, 113. (e) Sahai, R.; Morgan, L.; Rillema, D. P. *Inorg. Chem*. **1988**, *27*, 3495. (f) Sahai, R.; Rillema, D. P.; Shaver, R.; Van Wallendael, S.; Jackman, D. C.; Boldaji, M. *Inorg. Chem.* **1989**, *28*, 1022. (g) Rillema, D. P.; Sahai, R.; Mathews, P. T.; Edwards, A. K.; Shaver, R. J.; Morgan, L. *Inorg. Chem*. **1990**, *29*, 167.
(4) (a) Sahai, R.; Baucom, D. A.; Rillema, D. P. *Inorg. Chem.* **1986**, *25*, 3843. (b) Van Wallendael, S.; Shaver, R. J.; Rillema, D. P.; Yoblinski, B. J.; Stathis, M.; Guarr, T. *Inorg. Chem.* **1990**, *29*, 167.
(5) Barandu, T.; Song, X.; Lei, Y.; Endicott, J. F.; Van Wallendael, S.; Rillema, D. P. *J. Phys. Chem*. **1993**, *97*, 3225.
(6) Van Wallendael, S.; Perkovic, M. W.; Rillema, D. P. *Inorg. Chim. Acta* **1993**, *213*, 253.
(7) Boyde, S.; Strouse, G. F.; Jones, W. E., Jr.; Meyer, T. J. *J. Am. Chem. Soc.* **1990**, *112*, 7395.
(8) (a) Shaw, J. R.; Schmehl, R. H. *J. Am. Chem. Soc.* **1991**, *113*, 389. (b) Shaw, J. R.; Webb, R. T.; Schmehl, R. H. *J. Am. Chem. Soc*. **1990**, *112*, 1117.

S0020-1669(95)01344-9 CCC: $12.00

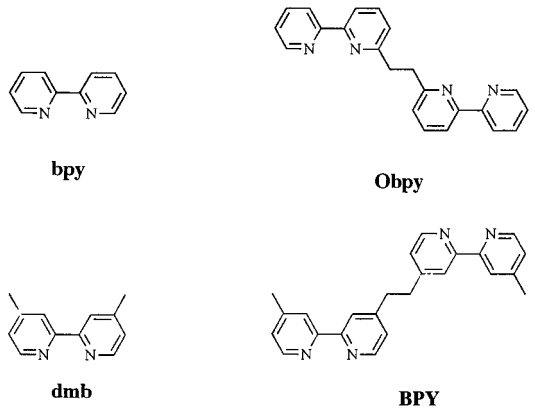

Figure 1. Ligands 2,2′-bipyridine (bpy), 4,4′-dimethyl-2,2′-bipyridine (dmb), 1,2-bis(2,2′-bipyridin-6-yl)ethane (Obpy), and 1,2-bis(4-methyl-2,2′-bipyridin-4′-yl) ethane (BPY).

in one case the dimethylene bridge is attached in the 6 position, in the other it is attached in the 4 position. Bimetallic complexes based on these two "isomers" are expected to exhibit the greatest difference in properties, since the ligand bridged in the 6 position is expected to be the most structurally distorted and, hence, would alter the physical and photophysical properties the most.

Experimental Section

Materials. $Ru(bpy)_2Cl_2$[9] (bpy = 2,2′-bipyridine) and $Ru(bpy)Cl_4$[10] were prepared according to previously published procedures. All solvents were HPLC grade. Tetrahydrofuran (THF) was distilled over sodium and benzophenone prior to use. Acetonitrile was dried over 3 Å activated molecular sieves prior to use. Commercially purchased tetrabutylammonium hexafluorophosphate (TBAH) was of electrometric grade (Southwestern Analytical, Inc.) and was used without further purification. All elemental analyses were performed by Atlantic Microlabs, Inc., Norcross, GA.

Preparation of Compounds. The synthesis of $[Ru(bpy)_2(BPY)](PF_6)_2$ (BPY = 1,2-bis(4-methyl-2,2′-bipyridin-4′-yl)ethane), $[\{Ru(bpy)_2\}_2(BPY)](PF_6)_4$, $[Ru(bpy)_2(dmb)](PF_6)_2$ (dmb = 4,4′-dimethyl-2,2′-bipyridine), and $[Ru(bpy)_3](PF_6)_2$ were previously reported[6] and were available for use in our laboratories. 1,2-Bis(2,2′-bipyridin-6-yl)ethane (Obpy) was prepared as previously reported.[11]

$[Ru(bpy)(Obpy)](PF_6)_2$. A solution consisting of 0.299 g (0.750 mmol) of $Ru(bpy)Cl_4$, 0.260 g (0.750 mmol) of Obpy, and 30 mL of ethylene glycol was prepared. The solution was placed under an Ar atmosphere and allowed to stir at reflux until the color of the solution changed from an initial brown to a deep orange-red. After several days, the reaction was quenched with 50 mL of distilled water and the product precipitated from the solution by dropwise addition of saturated aqueous NH_4PF_6. The product was purified by column chromatography (4 cm × 30 cm) packed with activated neutral alumina, Brockman Activity I. The ruthenium(II) hexafluorophosphate salt was eluted with acetone, precipitated with diethyl ether, collected by vacuum filtration, and dried overnight under vacuum. Anal. Calcd for $[Ru(bpy)(Obpy)](PF_6)_2$: C, 43.4; H, 2.97; N, 9.49. Found: C, 43.4; H, 2.96; N, 9.40.

$[Ru(bpy)_2(Obpy)](PF_6)_2$. A solution consisting of 0.20 g (0.384 mmol) of $Ru(bpy)_2Cl_2$, 0.19 g (0.768 mmol) of $AgPF_6$, and 50 mL of methanol was allowed to stir under an Ar atmosphere overnight. The solution was vacuum filtered to remove AgCl. The filtrate containing $[Ru(bpy)_2(MeOH)_2]^{2+}$ was then placed in a 250 mL side-arm addition funnel. A 4-fold excess of the ligand Obpy was dissolved in approximately 600 mL of methanol. The side-arm addition funnel was attached to the 1000 mL round-bottom flask containing the Obpy/methanol solution, and a condenser was then attached to the top of the side-arm addition funnel. As the Obpy/methanol solution refluxed, the methanol vapor was allowed to travel up the side arm of the addition funnel and condense into the addition funnel, thus diluting the $[Ru(bpy)_2(MeOH)_2]^{2+}$. After the addition funnel filled, the diluted $[Ru(bpy)_2(MeOH)_2]^{2+}$ trickled down the side arm and into the Obpy/methanol solution. The entire solution was allowed to reflux until the disappearance of the deep red color of $[Ru(bpy)_2(MeOH)_2]^{2+}$. Upon completion of the reaction, the methanol was removed with a rotary evaporator and the remaining orange powder was dissolved in a minimal amount of methylene chloride. The product was purified by column chromatography (4 cm × 20 cm) packed with neutral alumina, Brockman Activity I. Sequentially, methylene chloride served as the eluent for Obpy, acetonitrile served as the eluent for the monometallic $[Ru(bpy)_2(Obpy)]^{2+}$, and methanol served as the eluent for the bimetallic $[\{Ru(bpy)_2\}_2(Obpy)]^{4+}$. The acetonitrile was removed by rotary evaporation and the orange residue dissolved in a minimal amount of methylene chloride and reprecipitated from the solution with hexane. The monometallic product was filtered and vacuum dried. Anal. Calcd for $[Ru(bpy)_2(Obpy)](PF_6)_2$: C, 48.4; H, 3.30; N, 10.6. Found: C, 48.6; H, 3.41; N, 10.6.

$[\{Ru(bpy)_2\}_2(Obpy)](PF_6)_4 \cdot H_2O$. A solution of $[Ru(bpy)_2(MeOH)_2]^{2+}$ was prepared as described above. $[Ru(bpy)_2(MeOH)_2]^{2+}$ was added dropwise to a refluxing solution of $[Ru(bpy)_2(Obpy)](PF_6)_2$ dissolved in methanol. After the addition, the methanol was removed from the resulting solution by rotary evaporation and the residue was dissolved in distilled water. The bimetallic product was purified by column chromatography (5 cm × 40 cm) packed with cation exchange resin (Sephadex D-25, 40−120), swelled in distilled water, and eluted from the column with a 1.2 M NaCl solution. The desired product was precipitated from solution by the addition of solid NH_4PF_6, filtered, and redissolved in acetone to remove it from solid NaCl. After acetone was removed by evaporation using a rotary evaporator, the residue was dissolved in a minimal amount of methylene chloride, precipitated with hexane, filtered, and vacuum dried. Anal. Calcd for $[\{Ru(bpy)_2\}_2(Obpy)](PF_6)_4 \cdot H_2O$: C, 42.2; H, 2.92; N, 9.53. Found: C, 42.6; H, 3.05; N, 9.55.

Physical Measurements. Visible−UV spectra were recorded using a Perkin-Elmer Lambda Array 3840 UV/vis diode array spectrophotometer and an OLIS modified Cary 14 instrument. Room temperature solution spectra were obtained in methanol. Nuclear magnetic resonance spectra were obtained with a Varian X-300 NMR spectrometer.

Cyclic voltammograms were obtained in acetonitrile at room temperature using a PAR 173 potentiostat in conjunction with a PAR 175 universal programmer and were recorded using an IBM 7424 MT *X*/*Y*/*T* recorder. Measurements were made at a Pt-disk working electrode with a Pt counter electrode and 0.1 M TBAH as supporting electrolyte. Potentials were measured versus the saturated sodium chloride calomel electrode (SSCE). All samples were purged with nitrogen prior to measurement.

Room temperature and low-temperature emission spectra were obtained for each complex in a 4:1 ethanol:methanol mixture using a Spex Fluorolog 212 spectrofluorometer. All emission spectra were corrected for instrument response. Emission quantum yields (ϕ_{em}) were determined from an average of three freeze−pump−thaw degassed samples using techniques described previously.[12] Complexes were recrystallized from 4:1 ethanol:methanol prior to photophysical investigations. The following equation was used to calculate the emission quantum yields:[13]

$$\phi_{em} = (\eta^2_{cmpd}/\eta^2_{std})(A_{std}/A_{cmpd})(I_{cmpd}/I_{std})\phi_{std} \quad (1)$$

where A is the absorbance at the excitation wavelength, I is the integrated emission intensity, and η is the index of refraction of the solvent. Emission quantum yields were calculated relative to rhodamine B standard ($\phi_{std} = 0.71$)[14a] in 4:1 ethanol:methanol. All emission samples were prepared in HPLC grade, or better, solvents filtered through 0.45 μm PTFE filters, and then freeze−pump−thaw degassed prior to measurement. Excited-state lifetimes were determined by exciting the samples at 450 nm using an OPOTEK optical parametric

(9) Sullivan, B. P.; Salmon, D. J.; Meyer, T. J. *Inorg. Chem.* **1978**, *17*, 3334.
(10) Krause, R. A. *Inorg. Chem.* **1977**, *29*, 2863.
(11) Garber, T.; Van Wallendael, S.; Rillema, D. P.; Kirk, M.; Hatfield, W. E.; Welch, J. H.; Singh, P. *Inorg. Chem.* **1990**, *29*, 2863.
(12) Shaver, R. J.; Van Wallendael, S.; Rillema, D. P. *J. Chem. Educ.* **1991**, *68*, 604.
(13) Demas, J. N.; Crosby, G. A. *J. Phys. Chem.* **1971**, *75*, 991.

oscillator pumped by a frequency tripled Nd:YAG laser (Continuum Surlite, run at ≤1.5 mJ/10 ns pulse). Spectral regions were isolated using a Hamamatsu R955 photomultiplier tube (PMT) in a cooled housing (−15 °C, Amherst) coupled to an Acton SpectraPro 275 monochromator. Transients were recorded with a LeCroy 9359A digital oscilloscope (1 gigapoints/s). Oscilloscope control and data curve fitting were accomplished with a program developed in-house. Variable temperature emission lifetimes from 90 to 290 K were determined by adding a Cryo Industries EVT cryostat controlled by a Lakeshore 805 temperature controller to the system above. The cryostat was modified in-house by adding a larger copper thermal mass and then calibrated with an auxiliary thermocouple using ice water as the reference junction. This resulted in a temperature accuracy of ±1.6 K over the 90−290 K range. For temperatures above 290 K, the samples were equilibrated in a Fisher Isotemp bath and then transferred to the optical bench in a quartz dewar filled with bath water.

Photosubstitution Quantum Yields. Reinecke's salt, $KCr(NH_3)_2(NCS)_4$ with a quantum yield of 0.311, was used as the actinometer to evaluate the light source intensity.[14b] The preparation of Reinecke's salt was carried out in red light following literature procedures.[14b]

Two samples consisting of 0.0509 and 0.0710 g were dissolved in 10 mL of deionized water. Three 3-mL samples of each solution were transferred to 1 cm cuvettes for photolysis. The exposure times were 900, 1800, and 2400 s, respectively. Then 1 mL of the photolyzed solution was diluted to 10 mL by adding a solution of 0.1 M $Fe(NO_3)_3$ in 0.5 M $HClO_4$ to develop the reddish colored $[Fe(NCS)(H_2O)_5]^{2+}$ complex. The absorbances at 450 nm for both the photolyzed and a fresh sample kept in the dark were measured. The absorbance difference was used to determine the concentration of NCS^- produced from photolysis of Reinecke's salt. The light source intensity was then determined according to eq 2, where $\Delta n/\Delta t$ is the rate of NCS^-

$$I_0 = (\Delta n/\Delta t)/\phi_p(1 - 10^{-\epsilon cl}) \quad (2)$$

production, ϕ_p is the quantum yield (0.311), ϵ is the molar extinction coefficient of Reinecke's salt at 450 nm (31.2), C is the initial concentration of Reinecke's salt, and l is the light path length (1 cm). The light source intensity was determined to be $(1.76 \pm 0.39) \times 10^{-9}$ einsteins·s^{-1}.

Photosubstitution quantum yields of Ru^{II} complexes were measured in acetonitrile solutions containing 1 mM tetraethyl ammonium chloride ((TEA)Cl). Solution absorbances were adjusted to less than 0.1 at 450 nm, and then 3 mL was transferred to a 1 cm fluorescence cuvette and exposed to light at 450 nm. The emission intensities were recorded every second over 300−900 s during the photolysis process. The intensity changes were determined from plots of ΔI vs t, and the number of moles of compound photolyzed was then determined according to eq 3, where $\Delta n/\Delta t$ is the change in moles of the compound with time,

$$\Delta n/\Delta t = (\Delta I/\Delta t)(1/\kappa)(3/1000) \quad (3)$$

$\Delta I/\Delta t$ is the change in emission intensities with time at the emission wavelength maximum, κ is a coefficient from the emission calibration curve, and 3/1000 is a factor converting from concentration to moles. The photosubstitution quantum yield was then determined from eq 4.

$$\phi_p = (\Delta n/\Delta t)/I_0(1 - 10^{-\epsilon cl}) \quad (4)$$

For Ru^{II}(Obpy) complexes, the weak emission made it impossible to obtain reliable results by the above techniques. Thus, it was necessary to use absorption changes to obtain substitution quantum yields, but it was only possible to study photosubstitution in $[Ru(bpy)(Obpy)]^{2+}$ by this method due to the need of absorption data for the reaction product to determine the concentration changes. Samples with an absorbance of 0.43 were prepared for $[Ru(bpy)(Obpy)]^{2+}$. Three milliliters of each sample was transferred to a 1 cm cuvette and photolyzed for 1500 s. Then the absorption change with respect to a sample in the dark was measured and converted into the change in moles by correcting for the absorption of the $[Ru(Obpy)(CH_3CN)Cl]^+$ adduct[14c] to determine the quantum yield by eq 4.

Evaluation of Temperature Dependent Emission Data. The temperature dependent emission lifetimes obtained for each complex were plotted versus the absolute temperatures. The temperature dependent profiles generated for each complex were fitted to the following equations,[15,16] where $k_{obs} = 1/\tau$.

$$k_{obs} = [k_0' + k_1 \exp(-\Delta E_1/RT)]/[1 + \exp(-\Delta E_1/RT)] \quad (5)$$

$$k_{obs} = [k_0 + k_1 \exp(-\Delta E_1/RT) + k_2 \exp(-\Delta E_2/RT)]/[1 + \exp(-\Delta E_1/RT)] \quad (6)$$

A basic three-step strategy was used to fit the experimental data to both equations. Initial values for the variables k_0, k_1, k_2, ΔE_1, and ΔE_2 were obtained using the program "FLEXFIT". This program utilizes a simplex algorithm to determine approximate first "guesses" for each variable. Once the initial values were determined, the matrix routine in the FLEXFIT program[17] was used to further improve the initial guesses. However, this routine only allows the weighting of the "y" values. Therefore, once the improved initial values were obtained, a weighted nonlinear least squares dedicated program was used to further improve the values determined for each of the four variables. The weighted nonlinear least squares dedicated program allowed for weighting of both x and y values, using the standard deviations of the variables. The algorithm used in this program utilizes a set of normal equations as prescribed by Wentworth.[18] These normal equations were generated by taking the partial derivative of both equations with respect to each variable. Once performed, a set of four equations was generated, and from that the matrices used to improve the initial values were derived. Values for k_0, k_1, k_2, ΔE_1, and ΔE_2 were calculated until the weighted sum of the squares of the residuals were minimized. The standard deviation for the lifetimes were obtained from five measurements obtained at 30 s intervals at alternate temperatures. Computer fits were also obtained using the program ORIGIN.[19] Values of k_1, k_2, ΔE_1, and ΔE_2 determined using ORIGIN were within the experimental error limits found using the above algorithms; the values for k_0 were similar to k_{obs} found at 77 K.

Emission Spectral Fitting Parameters. Band shapes were calculated from the corrected emission spectra using spectral curve fitting parameters described by eq 7.

$$I(\hbar\omega) = I_\nu(\hbar\omega)/I_{00} - \sum_{\nu_i=0}\cdots\sum_{\nu_j=0}\{(E_{00} - \nu_i(\hbar\omega_i) - \ldots - \nu_j(\hbar\omega_j)/E_{00})^3(S_i^{\nu_i}/\nu_i!)\ldots(S_j^{\nu_j}/\nu_j!)\exp[-(4\ln 2)((\hbar\omega - E_{00} + \nu_i(\hbar\omega_i) + \ldots + \nu_j(\hbar\omega_j))/\Delta\nu_{1/2})^2]\} \quad (7)$$

The emission profiles were analyzed by a two-mode, temperature dependent Franck−Condon analysis based on the parameters E_{00}, $S_{i\rightarrow j}$ (1 and 2), $\hbar\omega_{i\rightarrow j}$ (1 and 2) and $\Delta\nu_{1/2}$. In the equation, E_{00} is the zero−zero energy, $S_{i\rightarrow j}$ and $\hbar\omega_{i\rightarrow j}$ are respectively the electron-vibrational coupling constant and vibrational spacing between vibrational frequency modes that vary in energy from medium- to low-energy frequency vibrations, $\Delta\nu_{1/2}$ is the full width at half maximum for the individual vibronic contributors, and $\hbar\omega$ is the frequency of observation.

Molecular Modeling Calculations. MM2 calculations were performed using PCModel Version 3.0, by Serena Software. The force field used in the calculations was MMX, which is derived from the MM2 force field (QCPE-395, 1977) of N. L. Allinger. It differs from Allinger's force field in that the MMX force field has the ability to handle more atom types, transition metals and transition states and has more parameters in its data base.

(14) (a) Calvert, J. G. *Photochemistry*; Wiley: New York, 1966. (b) Wegner, E. E.; Adamson, A. W. *J. Am. Chem. Soc.* **1966**, *88*, 394. (c) The compound $[Ru(Obpy)(CH_3CN)Cl](PF_6)$ was prepared independently by the reaction of $RuCl_3$ with Obpy in the presence of LiCl. It was isolated as the PF_6^- salt.

(15) Allsopp, S. R.; Cox, A.; Kemp, J. T.; Reed, W. J. *J. Chem. Soc., Faraday Trans. 1* **1978**, *74*, 1275.

(16) Kober, E. M.; Caspar, J. V.; Lumpkin, R. S.; Meyer, T. J. *J. Phys. Chem.* **1986**, *90*, 3722.

(17) Copyright: Ramette, R. W. Carlton College, 1988.

(18) Wentworth, W. E. *J. Chem. Educ.* **1965**, *42*, 96, 162.

(19) *ORIGIN*, Version 2.94; MicroCal Software: Northampton, MA, 1991−3.

The Ru−N bonds were not externally parametrized in any way, although the oxidation state of ruthenium and its covalent radius (1.355 Å for Ru^{II} per manual) were used in the calculation. To prevent falling into a trap of a local minimum, each structure was placed in a randomizing routine after initial minimization. This was performed iteratively for *each atom movement.* Once complete, the structure with the minimum energy (via randomization) was displayed. The initial minimizations and the randomizations were done in triplicate, and each time the minimum energies were within approximately 1% of each other.

Results

Preparation of Compounds. The preparation of the monometallic $[Ru(bpy)_2(Obpy)]^{2+}$ and the bimetallic $[\{Ru(bpy)_2\}_2(Obpy)]^{4+}$ complexes followed previously reported strategies[20] utilizing the lability of the coordinated solvent molecules of the intermediate $[Ru(bpy)_2(CH_3OH)_2]^{2+}$. The methanolate species proved to be a convenient intermediate since the preparative reactions were carried out in methanol. Upon addition of this intermediate to a solution containing the ligand Obpy, substitution of the two solvent molecules by one of the ligand's open bidentate sites occurred. Formation of the bimetallic complex was favored with a 2:1 ratio of $[Ru(bpy)_2(CH_3OH)_2]^{2+}$ to Obpy, while the formation of $[Ru(bpy)_2(Obpy)]^{2+}$ was favored with $[Ru(bpy)_2(CH_3OH)_2]^{2+}$ in a large excess of Obpy. Formation of $[Ru(bpy)_2(Obpy)]^{2+}$ was enhanced by controlling the addition of a dilute solution of $[Ru(bpy)_2(CH_3OH)_2]^{2+}$ to a solution of Obpy. In both cases, mixtures of $[Ru(bpy)_2(Obpy)]^{2+}$ and $[\{Ru(bpy)_2\}_2(Obpy)]^{2+}$ were obtained and purification was necessary. The monometallic complex was purified on a neutral alumina column, whereas cation exchange chromatography was used to purify the bimetallic species.

The NMR spectra of the methyl and methylene proton resonances proved to be good signatures for the complexes. The methyl proton resonances of the free ligands dmb and BPY shifted downfield from 2.42^s to 2.55^s ppm and 2.43^s to 2.55^s ppm, respectively, upon coordination to ruthenium. The resonance for the methyl protons of the uncoordinated bpy unit of $[Ru(bpy)_2BPY]^{2+}$ remained at 2.44^s ppm. The methylene protons of the BPY complexes responded in like manner. The proton resonance of BPY shifted from 3.16^s to 3.22^s ppm for $[\{Ru(bpy)_2\}_2(BPY)]^{4+}$; for $[Ru(bpy)_2(BPY)]^{2+}$, the proton resonances of the methylene group adjacent to ruthenium occurred at 3.29^s ppm, and for the other methylene protons, the resonance was observed at 3.18^s ppm. The chemical shifts of methylene protons for the Obpy complexes were more complicated due to structural effects. Proton chemical shifts occurred both downfield and upfield, depending on the proton environment. The protons affected by anistropic ring currents due to orthogonally oriented ligands were shifted upfield due to greater shielding from electron density on ruthenium; the other proton resonances were shifted downfield in agreement with the observations noted above. Further, the two methylene protons resulting in the downfield resonance were no longer equivalent and the signal was split into two multiplets. The resonance for Obpy was found at 3.42^s ppm and the resonances for the Obpy complexes were observed at 3.85^M, 3.61^M, and 3.15^M ppm for $[Ru(bpy)(Obpy)]^{2+}$, at 3.27^M, 3.06^M, and 2.51^M ppm for $[Ru(bpy)_2(Obpy)]^{2+}$, and at 3.62^s and 2.54^M ppm for $[\{Ru(bpy)_2\}_2(Obpy)]^{4+}$. The proton splitting patterns for the Obpy complexes could be attributed to the *antimeso* configuration of the methylene protons, particularly for $Ru(bpy)(Obpy)]^{2+}$.

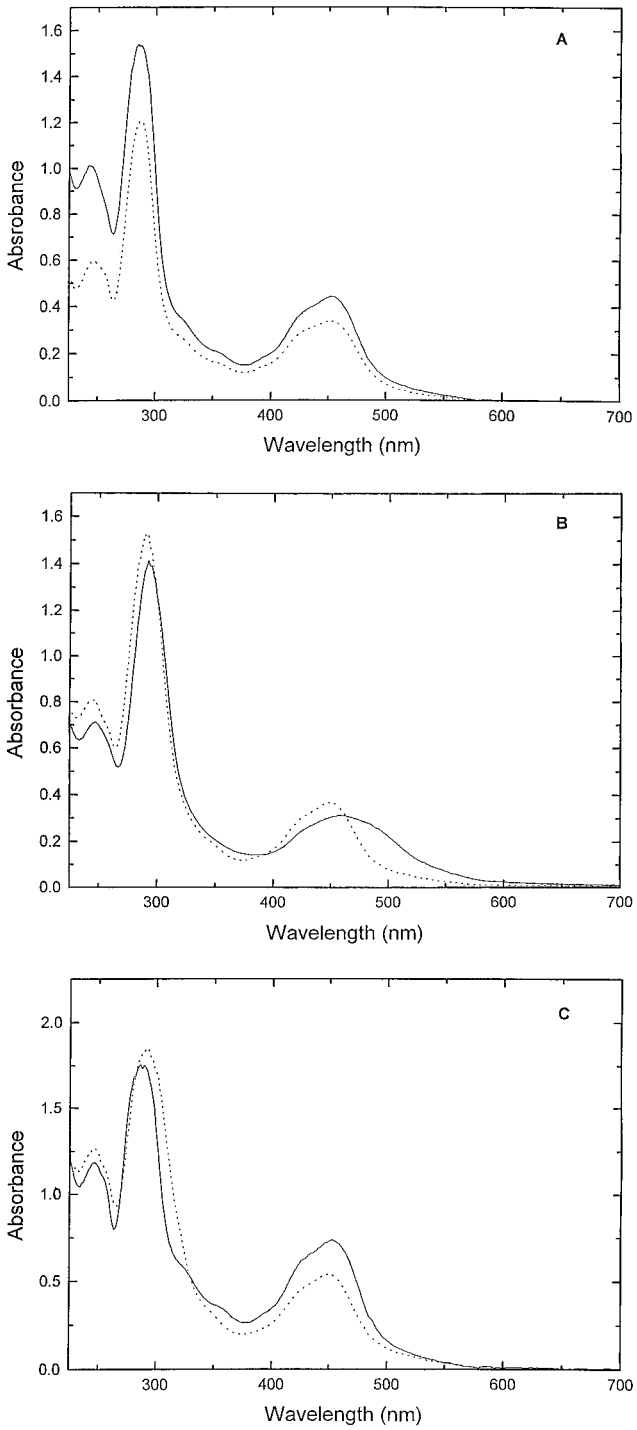

Figure 2. Absorption spectra of the complexes in methanol. The concentrations were 3.5×10^{-5} M; the cell path length was 1 cm. (A) $[Ru(bpy)_2(dmb)]^{2+}$ (···), $[Ru(bpy)_2(BPY)]^{2+}$ (—), (B) $[Ru(bpy)_2(Obpy)]^{2+}$ (···), $[Ru(bpy)(Obpy)]^{2+}$ (—), (C) $[\{Ru(bpy)_2\}_2(Obpy)]^{4+}$ (···), $[\{Ru(bpy)_2\}_2(BPY)]^{4+}$ (—).

Absorption Properties. The absorption spectra are illustrated in Figure 2 and absorption data listing energy maxima and absorption coefficients are summarized in Table 1. Two distinct sets of absorption bands were present for all of the complexes. As previously reported for analogous systems,[6,21] the set at higher energy can be attributed to intraligand $\pi \rightarrow \pi^*$

(20) (a) Kalyanasundaram, K.; Nazeeruddin, M. K.; Gratzel, M.; Viscardi, G.; Savarino, P.; Barni, E. *Inorg. Chim. Acta* **1992**, *198*, 831. (b) Collin, J.; Beley, M.; Sauvauge, J. P.; Barigelletti, F. *Inorg. Chim. Acta* **1991**, *45*, L183. (c) Haga, M. A. *Inorg. Chim. Acta* **1987**, *17*, 2660. (d) Dose, E. V.; Wilson, L. *Inorg. Chem.* **1978**, *17*, 2660. (e) Hunziker, M.; Ludi, A. *J. Am. Chem. Soc.* **1977**, *99*, 7370.

(21) Crutchley, R. J.; Lever, A. B. P. *Inorg. Chem.* **1986**, *21*, 2276.

Table 1. Absorption Data for Ru^{II}(Obpy) and Ru^{II}(BPY) Complexes[a]

complex	λ_{max} (nm) ($\epsilon \times 10^{-4}$ ($M^{-1}\cdot cm^{-1}$))					
$[Ru(bpy)(Obpy)]^{2+}$ [b]	248 (1.60)		293 (3.40)			455 (0.84)
$[Ru(bpy)_2(Obpy)]^{2+}$ [b]	244 (2.17)	256 (2.39)	291 (4.98)		350 (0.53)	449 (1.27)
$[\{Ru(bpy)_2\}_2(Obpy)]^{4+}$ [b]	246 (3.55)	258 (2.39)	291 (8.47)		353 (0.72)	450 (1.69)
$[Ru(BPY)_3]^{2+}$ [c]	238 (3.00)	250 (2.50)	285 (8.70)	323 (0.65)	345 (0.65)	450 (1.49)
$[Ru(bpy)_2(BPY)]^{2+}$ [d]	246 (2.74)		288 (5.32)	327 (0.90)	354 (0.55)	453 (1.34)
$[\{Ru(bpy)_2\}_2(BPY)]^{4+}$ [b]	246 (3.20)		286 (6.15)	326 (1.57)	355 (0.96)	454 (1.98)
$[Ru(bpy)_2(dmb)]^{2+}$ [e]	247 (2.03)		289 (5.32)	324 (0.84)	355 (0.46)	454 (1.09)

[a] $\lambda_{max} \pm 2$ nm; $T = 298$ K; 1 cm path length. [b] In methanol. [c] Reference 21. [d] In ethanol. [e] In CH_2Cl_2.

Table 2. Integration Data for Ru^{II}(Obpy) and Ru^{II}(BPY) Complexes[a]

complex	λ_{max} (nm)	area (M^{-1})	area ratio[b]	fwhm (nm)	fwhm ratio[b]	ϵ ratio[b]
$[Ru(bpy)(Obpy)]^{2+}$	452	0.1050	0.77	116	1.52	0.56
$[Ru(bpy)_2(Opby)]^{2+}$	450	0.1067	0.78	73.5	0.96	0.85
$[\{Ru(bpy)_2\}_2(Obpy)]^{4+}$ [c]	450	0.1352	0.99	75.0	0.98	1.13
$[Ru(bpy)_3]^{2+}$	452	0.1363	1.00	76.5	1.00	1.00
$[Ru(bpy)_2(BPY)]^{2+}$	452	0.1094	0.80	75.0	0.98	0.90
$[\{Ru(bpy)_2\}_2(BPY)]^{4+}$ [d]	452	0.1755	1.29	76.5	1.00	1.32
$[Ru(bpy)_2(dmb)]^{2+}$	452	0.0951	0.70	76.5	1.00	0.73

[a] In methanol; concentration $= 3.5 \times 10^{-5}$ M. Integration from 375 to 600 nm. [b] Ratios per molecule with respect to $[Ru(bpy)_3]^{2+}$. [c] Per Ru^{II} metal; area ratio = 0.50; ϵ ratio = 0.50. [d] Per Ru^{II} metal; area ratio = 0.65; ϵ ratio = 0.50.

transitions; the set at lower energy can be assigned as metal-to-ligand charge transfer, $d\pi(Ru^{II}) \rightarrow \pi^*$(bpy), transitions.

The positions and shapes of the $\pi \rightarrow \pi^*$ transitions do not differ greatly between the complexes. This is reasonable since the ligands are basically the same, bipyridine and/or "methyl substituted bipyridine". The number of bipyridine units per molecule, however, does change, and this is reflected in the values of the absorption coefficients. Thus, the absorption coefficients increase in the series $[Ru(bpy)(Obpy)]^{2+} < [Ru(bpy)_2(Obpy)]^{2+} < [\{Ru(bpy)_2\}_2(Obpy)]^{4+}$, approximately in the ratio 1:1.3:2 as expected for the transitions with maxima near 245 and 291 nm.

The $d\pi(Ru^{II}) \rightarrow \pi^*$(bpy) transitions occurred near 450 nm. The absorption coefficients of the complexes in this region differed, increasing in the order $[Ru(bpy)(Obpy)]^{2+} < [Ru(bpy)_2(dmb)]^{2+} < [Ru(bpy)_2(Obpy)]^{2+} < [Ru(bpy)_2(BPY)]^{2+} < [Ru(bpy)_3]^{2+} < [\{Ru(bpy)_2\}_2(Obpy)]^{4+} < [\{Ru(bpy)_2\}_2(BPY)]^{4+}$. However, as noted in Figure 2, the $d\pi(Ru^{II}) \rightarrow \pi^*$(bpy) absorption manifold of the $[Ru(bpy)(Obpy)]^{2+}$ complex is broader than the others. Thus, in order to compare intensities of the $d\pi(Ru^{II}) \rightarrow \pi^*$(bpy) transitions for the various complexes, numerical integrations of the absorption manifolds from 375 to 600 nm were performed.[22] The integrated areas, absorption coefficients, and ratios are listed in Table 2.

Comparison of the area ratios with $[Ru(bpy)_3]^{2+}$ as the standard[20] give numbers less than 1 for all the complexes except for $[\{Ru(bpy)_2\}_2(BPY)]^{2+}$, which has a value of 1.29. The fact that $[Ru(bpy)_2(dmb)]^{2+}$ and $[Ru(bpy)(Obpy)]^{2+}$ have 7/10 to 8/10 of the oscillator strength of $[Ru(bpy)_3]^{2+}$ for this transition suggests that each should be chosen as standards for their respective series. Then the area ratios for the series $[Ru(bpy)_2(dmb)]^{2+}$, $[Ru(bpy)_2(BPY)]^{2+}$, and $[\{Ru(bpy)_2\}_2(BPY)]^{4+}$ are 1:1.15:1.85, respectively, and, for the series $[Ru(bpy)(Obpy)]^{2+}$, $[Ru(bpy)_2(Obpy)]^{2+}$, and $[Ru(bpy)_2\}_2(Obpy)]^{4+}$ are 1:1.02:1.29. When compared to area ratios, ratios for the BPY series were similar. A similar comparison for the Obpy series differs due to the different band shape of the $[Ru(bpy)_2(Obpy)]^{2+}$ complex compared to the others in the series.

Table 3. Electrochemical Data for Ru^{II}(Obpy) and Ru^{II}(BPY) Complexes[a]

complex	E_{ox} (ΔE_p (mV))		E_{red} (ΔE_p (mV))	
$[Ru(bpy)(Obpy)]^{2+}$	1.29 (61)	−1.32 (60)	−1.48 (61)	−1.78 (62)
$[Ru(bpy)_2(Obpy)]^{2+}$	1.35 (60)	−1.33 (63)	−1.55 (61)	−1.81 (61)
$[\{Ru(bpy)_2\}_2(Obpy)]^{4+}$	1.32 (64)	−1.33 (61)	−1.54 (62)	−1.81(61)
$[Ru(bpy)_3]^{2+}$	1.27 (60)	−1.31 (62)	−1.50 (60)	−1.77 (62)
$[Ru(bpy)_2(BPY)]^{2+}$	1.24 (68)	−1.35 (61)	−1.56 (60)	−1.93 (61)
$[\{Ru(bpy)_2\}_2(BPY)]^{4+}$	1.28 (65)	−1.32 (61)	−1.53 (62)	−1.91 (62)
$[Ru(bpy)_2(dmb)]^{2+}$	1.25 (58)	−1.30 (62)	−1.56 (60)	−1.96 (61)

[a] All potentials in volts vs SSCE; in CH_3CN; 0.10 M TBAH; scan rate = 200 mV·s^{-1}; $T = 298$ K.

Electrochemistry. Oxidation and reduction potentials of the Ru^{II}(Obpy) and Ru^{II}(BPY) complexes were determined by cyclic voltammetry. The cyclic voltammograms over the −2.0 to +2.0 V (vs SSCE) region consisted of four reversible processes, one oxidation and three closely spaced reductions. The reversibility was noted by the anodic to cathodic current ratio of near 1 and the ΔE_p values near 59 mV for a specific redox process. $E_{1/2}$ and ΔE_p values are listed in Table 3.

The oxidations fall within the 1.25−1.35 V range and correspond to removal of an electron from the d orbital of Ru^{II} to give Ru^{III}. The bimetallic complexes also exhibited one oxidation with a ΔE_p value of 64 ± 2 mV, but the peak currents were twice that of $[Ru(bpy)_3]^{2+}$ in equal molar solutions, indicating that the oxidation of the bimetallic complexes was a two one-electron process. Since the accepted ΔE_p value for a reversible process is $59/n$, where n is the number of electrons transferred,[23] it follows that the oxidation of the bimetallic species consists of two closely spaced waves accounting for the two-electron nature of the oxidation process.

The reductions can be attributed to a sequential process associated with the reduction of each bidentate ligand. The first reduction occurred at -1.31 ± 0.04 V for all of the complexes, whereas the third reduction of the BPY complexes was shifted by nearly 0.2 V in the negative direction from the one for $[Ru(bpy)_3]^{2+}$ (−1.77 V). The pattern is in keeping with initial reduction of bipyridine followed by reduction of the bipyridine ligands bearing electron-donating methyl substituents.

The sequence of reductions are noted in eqs 8−10 using $[Ru(bpy)_2(Obpy)]^{2+}$ as an example.

$$Ru^{II}(bpy)(bpy)(Obpy)^{2+} + e^- \rightarrow Ru^{II}(bpy^{\bullet -})(bpy)(Obpy)^{+} \quad (8)$$

$$Ru^{II}(bpy^{\bullet -})(bpy)(Obpy)^{+} + e^- \rightarrow Ru^{II}(bpy^{\bullet -})(bpy^{\bullet -})(Obpy)^{0} \quad (9)$$

$$Ru^{II}(bpy^{\bullet -})(bpy^{\bullet -})(Obpy)^{0} + e^- \rightarrow Ru^{II}(bpy^{\bullet -})(bpy^{\bullet -})(Obpy^{\bullet -})^{-1} \quad (10)$$

(22) The program ORIGIN was used for the integration.

(23) Nicholson, R. S.; Shain, I. *Anal. Chem.* **1964**, *36*, 705.

Table 4. Emission Data for Ru^{II}(Obpy) and Ru^{II}(BPY) Complexes at 77 and 298 K[a]

	77 K		298 K			
complex	λ_{max} (nm)	τ (μs)	λ_{max} (nm)	Φ_{em}[b]	τ (s)	$\Phi_p \times 10^3$ [c]
$[Ru(bpy)(Obpy)]^{2+}$	577 ± 2	7.7 ± 0.3	598 ± 3	$(3.6 \pm 0.2) \times 10^{-4}$	$(3.0 \pm 2.9) \times 10^{-9}$ [d]	12 ± 1[e]
$[Ru(bpy)_2(Obpy)]^{2+}$	575 ± 2	5.2 ± 0.1	603 ± 3	$(2.3 \pm 0.1) \times 10^{-4}$	$(2.6 \pm 1.3) \times 10^{-9}$ [d]	
$[\{Ru(bpy)_2\}_2(Obpy)]^{4+}$	582 ± 2	5.5 ± 0.4	605 ± 3	$(2.6 \pm 0.04) \times 10^{-4}$	$(2.6 \pm 2.8) \times 10^{-9}$ [d]	
$[Ru(bpy)_3]^{2+}$	576 ± 2	5.2 ± 0.2	598 ± 3	$(9.2 \pm 0.6) \times 10^{-2}$	$(5.8 \pm 0.3) \times 10^{-7}$	4.2 ± 0.4[f]
$[Ru(bpy)_2(BPY)]^{2+}$	581 ± 2	4.8 ± 0.1	604 ± 3	$(7.8 \pm 0.7) \times 10^{-2}$	$(7.4 \pm 0.5) \times 10^{-7}$	1.8 ± 0.6[f]
$[\{Ru(bpy)_2\}_2(BPY)]^{4+}$	583 ± 2	4.7 ± 0.1	610 ± 3	$(7.9 \pm 0.3) \times 10^{-2}$	$(7.7 \pm 0.6) \times 10^{-7}$	1.6 ± 0.3[f]
$[Ru(bpy)_2(dmb)]^{2+}$	583 ± 2	4.7 ± 0.1	607 ± 3	0.11 ± 0.003	$(7.5 \pm 0.4) \times 10^{-7}$	3.8 ± 0.3[f]

[a] In 4:1 ethanol:methanol unless indicated otherwise; at 77 K, $\lambda_{ex} = 450$ nm; at 298 K, $\lambda_{ex} = 449-456$ nm. [b] Relative to rhodamine B base, $\Phi_{em} = 0.71$ at 298 K. [c] In 1 mM (TEA)Cl acetonitrile solution, $\lambda_{ex} = 450$ nm. [d] Values were extrapolated from the k vs T plot. [e] Concentration changes determined by absorption changes. [f] Concentration changes determined by emission intensity changes.

Emission Properties at 77 and 298 K. The emission spectra of the complexes at 298 K were broad and unstructured, while the ones at 77 K displayed vibrational components similar to those reported for emission from $[Ru(bpy)_3]^{2+}$.[24] The positions of the first vibrational maximum obtained at 77 K and the emission maxima obtained in fluid solution at room temperature are tabulated in Table 4. The energy maxima shift 23 ± 3 nm from ~580 to ~603 nm upon changing from the glassy matrix at 77 K to fluid solution at room temperature. At 77 K, the positions of the emission energy maxima are relatively constant, but more systematic changes are observed at room temperature where emission energies fall in the series $[Ru(bpy)(Obpy)]^{2+}$ (598 nm) > $[Ru(bpy)_2(Obpy)]^{2+}$ (603 nm) > $[\{Ru(bpy)_2\}_2(Obpy)]^{4+}$ (605 nm) and $[Ru(bpy)_2(BPY)]^{2+}$ (604 nm) > $[\{Ru(bpy)_2\}_2(BPY))]^{4+}$ (610 nm).

Emission decays were monoexponential at both 77 and 298 K, and the results are tabulated in Table 4. The emission lifetimes were approximately an order of magnitude larger in the glassy matrix at 77 K compared to fluid solution at room temperature (~5 μs vs ~0.7 μs) for the BPY complexes but 3 orders of magnitude larger at 77 K compared to fluid solution at room temperature (~5 μs vs ~3 ns) for the Obpy complexes. This variation is consistent with the metal-to-ligand charge transfer nature of the process where solvent plays a critical role in responding to the photoinduced dipole change and thereby facilitating relaxation to the ground state.[25] At 77 K, the emission lifetimes of the Ru^{II}(Obpy) complexes on an average are longer than the one for $[Ru(bpy)_3]^{2+}$ (5.2 μs), while those of the Ru^{II}(BPY) series are less. At 298 K, however, the opposite is true, the Ru^{II}(BPY) complexes on an average have longer emission lifetimes than $[Ru(bpy)_3]^{2+}$, while those of the Ru^{II}(Obpy) series are less. Clearly, the deactivating channels at room temperature alter the emission behavior from that observed at 77 K.

The emission quantum yields for the complexes were determined relative to rhodamine B (0.71)[14] at room temperature in a 4:1 ethanol:methanol mixture and varied from 10^{-2} to 10^{-4} (Table 4). The ones for the Ru^{II}(Obpy) complexes decreased in the order $[Ru(bpy)(Obpy)]^{2+}$ (3.6×10^{-4}) > $[Ru(bpy)_2(Obpy)]^{2+}$ (2.3×10^{-4}) ~ $[\{Ru(bpy)_2\}_2(Obpy)]^{4+}$ (2.6×10^{-4}), while for the Ru^{II}(BPY) series the order was $[Ru(bpy)_2(BPY)]^{2+}$ (7.8×10^{-2}) ~ $[\{Ru(bpy)_2\}_2(BPY)]^{4+}$ (7.9×10^{-2}). Relative to $[Ru(bpy)_3]^{2+}$, ϕ_{em} for the Ru^{II}(BPY) series were roughly equivalent, whereas for the Ru^{II}(Obpy) series ϕ_{em} was over 2 orders of magnitude smaller. Thus, ϕ_{em} differs markedly when both series are compared together, but within each series, the trends are in agreement with the energy gap law as noted by shifts in emission energy maxima.

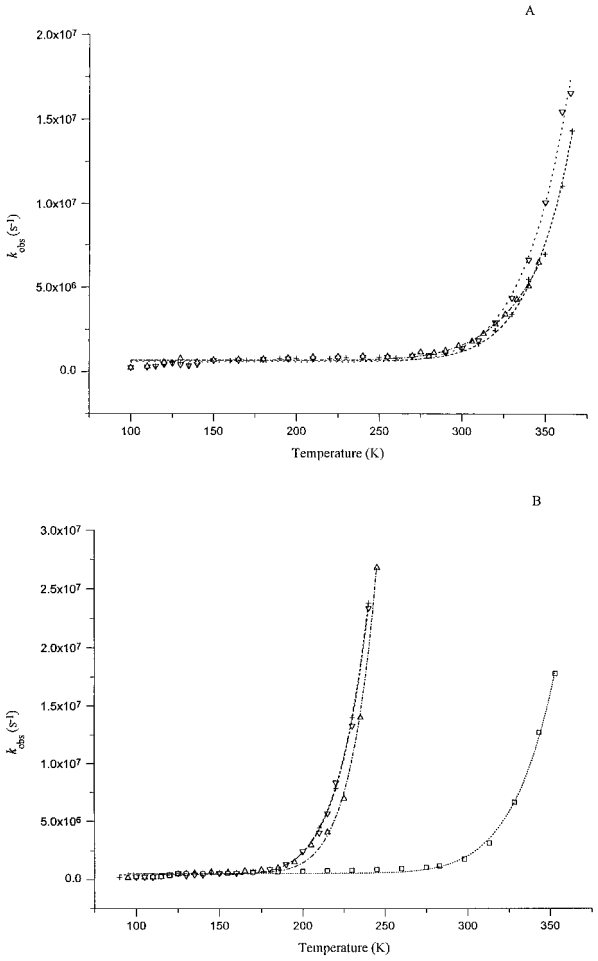

Figure 3. Temperature dependent emission lifetimes of (A) (▽) $[Ru(bpy)_2(BPY)]^{2+}$, (+) $[\{Ru(bpy)_2\}_2(BPY)]^{4+}$, and (△) $[Ru(bpy)_2(dmb)]^{2+}$ in 4:1 ethanol:methanol. (B) (□) $[Ru(bpy)_3]^{2+}$, (+) $[Ru(bpy)_2(Obpy)]^{2+}$, (△) $[Ru(bpy)(Obpy)]^{2+}$, and (▽) $[\{Ru(bpy)_2\}_2(Obpy)]^{4+}$ in 4:1 ethanol:methanol. The experimental points were fit to eq 6.

Photosubstitution Quantum Yields. Photosubstitution was studied for the complexes and compared to the one obtained for $[Ru(bpy)_3]^{2+}$. The photosubstitution quantum yields are tabulated in Table 4 and ranged from 12×10^{-3} to 5.8×10^{-3} for chloride ion replacement of one of the bidentate ligands. The order was $[Ru(bpy)(Obpy)]^{2+}$ >> $[Ru(bpy)_3]^{2+}$ > $[Ru(bpy)_2(dmb)]^{2+}$ > $[Ru(bpy)_2(BPY)]^{2+}$ > $[\{Ru(bpy)_2\}_2(bpy)]^{4+}$.

Temperature Dependent Emission Lifetimes. Figure 3 shows the temperature dependence of the emission lifetimes for the complexes in 4:1 ethanol:methanol over the 90−360 K

(24) (a) Hager, G. D.; Crosby, G. A. *J. Am. Chem. Soc.* **1975**, *97*, 7031. (b) Hager, G. D.; Watts, R. J.; Crosby, G. A. *J. Am. Chem. Soc.* **1975**, *97*, 7037.

(25) (a) Kim, H.-B.; Kitamura, H.; Tazuke, S. *J. Phys. Chem.* **1990**, *94*, 1414. (b) Milder, S. J. *Inorg. Chem.* **1989**, *28*, 868. (c) Kitamura, N.; Sato, J.; Kim, H.-B.; Obota, R.; Tazuke, S. *Inorg. Chem.* **1988**, *27*, 651. (d) Kober, E. M.; Sullivan, B. P.; Meyer, T. J. *Inorg. Chem.* **1984**, *23*, 2098. (e) Caspar, J. V.; Meyer, T. J. *J. Am. Chem. Soc.* **1983**, *105*, 5583.

Table 5. Temperature Dependence of Emission Lifetime[a]

complex	$k_0 \times 10^{-5}$ (s^{-1})	$k_1 \times 10^{-5}$ (s^{-1})	$k_2 \times 10^{-13}$ (s^{-1})	ΔE_1 (cm^{-1})	$\Delta E_2 \times 10^{-3}$ (cm^{-1})
$[Ru(bpy)(Obpy)]^{2+}$	3.40 ± 0.14	23.0 ± 4.1	5.29 ± 2.90	201 ± 19	2.47 ± 0.08
$[Ru(bpy)_2(Obpy)]^{2+}$	1.14 ± 0.22	15.7 ± 1.9	3.55 ± 1.05	122 ± 12	2.37 ± 0.05
$[\{Ru(bpy)_2\}_2(Obpy)]^{4+}$	1.25 ± 0.19	36.8 ± 13.8	4.33 ± 2.72	241 ± 43	2.42 ± 0.09
$[Ru(bpy)_3]^{2+}$	1.38 ± 0.24	24.1 ± 0.4	13.0 ± 10.7	200 ± 3	3.91 ± 0.17
$[Ru(bpy)_2(BPY)]^{2+}$	2.20 ± 0.11	11.6 ± 0.5	47.8 ± 18.3	101 ± 5	4.32 ± 0.08
$[\{Ru(bpy)_2\}_2(BPY)]^{4+}$	2.45 ± 0.18	11.4 ± 0.6	8.73 ± 3.32	111 ± 7	3.99 ± 0.09
$[Ru(bpy)_2(dmb)]^{2+}$	1.24 ± 0.07	13.8 ± 0.1	1.95 ± 0.55	100 ± 7	3.69 ± 0.06

[a] In 4:1 ethanol:methanol, $\lambda_{ex} = 450$ nm.

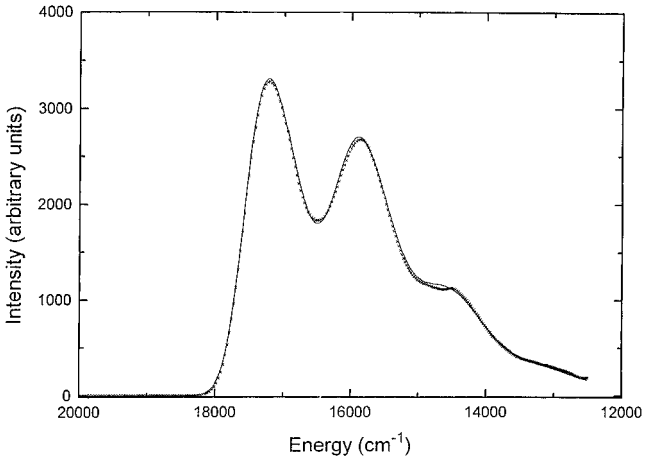

Figure 4. Corrected emission spectrum of $[\{Ru(bpy)_2\}_2(Obpy)]^{4+}$ (×) in a 4:1 ethanol:methanol glass at 85 K. The spectrum was calculated (—) using the parameters in Table 6.

range. Starting at 90 K, the emission lifetimes of a specific complex remain nearly the same in the glassy matrix up to ~110 K. Between 110 and 130 K, the glass-to-fluid region, emission lifetimes decrease rather rapidly. Above 150 K in the fluid region, lifetimes again decrease slowly until 190 K for Obpy complexes and 300 K for BPY complexes where once again marked changes in lifetimes occur.

The temperature dependent lifetime behavior was fit to eq 6, and the results are tabulated in Table 5. According to the data in Table 5, k_1 varied from 1.1×10^6 to 3.7×10^6 s^{-1}, k_2 varied from 1.95×10^{13} to 4.7×10^{14} s^{-1}, ΔE_1 varied from 100 to 241 cm^{-1}, and ΔE_2 varied from 2370 to 4320 cm^{-1}. The values of k_0 are consistent with emission lifetimes at 77 K reported in Table 4. The extrapolated values ranged from 3 to 9 μs compared to 5 to 7 μs at 77 K. The k_1, k_2, ΔE_1 and ΔE_2 values are consistent with those previously reported for other ruthenium(II) diimine complexes.

Emission Spectral Fitting Parameters. The emission spectrum of $[\{Ru(bpy)_2\}_2(Obpy)]^{4+}$ at 85 K is shown in Figure 4 along with the results of a spectral curve fitting program described earlier[16,26] based on the parameters E_{00}, $\hbar\omega_1$, $\hbar\omega_2$, S_1, S_2 and $\Delta\nu_{1/2}$. E_{00} is the zero−zero energy, $\hbar\omega$ is the frequency of a medium- and low-energy vibrational mode, S is related to the change in equilibrium displacement between the ground and excited states (ΔQ_{eq}) by $S = {}^1/_2(M\omega/\hbar)(Q)^2$, where M is the reduced mass and ω is the angular frequency, and $\Delta\nu_{1/2}$ is the full width at half-maximum for the individual vibronic contributors. In the emission spectrum illustrated in Figure 4, vibrational progressions can be seen at 77 K giving good initial estimates for E_{00} and $\hbar\omega_1$. S_1 was readily estimated from the peak heights of the first two components. For a satisfactory fit, both $\hbar\omega_2$ and S_2 must be included, even though $\hbar\omega_2$ progressions were not experimentally observed. Both parameters were varied for $[\{Ru(bpy)_2\}_2(Obpy)]^{4+}$ resulting in $\hbar\omega_2 = 393$ cm^{-1} and $S_2 = 0.87$ which are consistent with those reported for related compounds.[27] The best fit values for the parameters obtained for the series of compounds are summarized in Table 6.

Table 6. Emission Data and Emission Spectral Fitting Parameters in 4:1 Ethanol:Methanol (v:v) Glasses[a]

complex	E_{00} (cm^{-1})	$\hbar\omega_1$ (cm^{-1})	S_1	$\hbar\omega_2$ (cm^{-1})	S_2	$\Delta\nu_{1/2}$
$[Ru(bpy)(Obpy)]^{2+}$	17350	1372	1.03	431	1.02	565
$[Ru(bpy)_2(Obpy)]^{2+}$	17396	1361	1.06	404	0.97	559
$[\{Ru(bpy)_2\}_2(Obpy)]^{4+}$	17370	1347	1.08	393	0.87	618
$[Ru(bpy)_3]^{2+}$	17252	1359	1.05	383	0.97	598
$[Ru(bpy)_2(BPY)]^{2+}$	17192	1364	1.07	409	0.94	580
$[\{Ru(bpy)_2\}_2(BPY)]^{4+}$	17364	1359	1.03	412	0.89	599
$[Ru(bpy)_2(dmb)]^{2+}$	17215	1364	1.02	406	1.04	536

[a] Error limits are as follows: temperature ± 2 K; E_{00} ± 10 cm^{-1}; $\hbar\omega$ ± 10 cm^{-1}; S ± 2%; $\Delta\nu_{1/2}$ ± 5%.

Within the series of compounds, the E_{00}, $\hbar\omega_1$, $\hbar\omega_2$, S_1, S_2, and $\Delta\nu_{1/2}$ values were similar. Thus, $E_{00} \cong 17\,300 \pm 110$ cm^{-1}, $\hbar\omega_1 \cong 1360 \pm 12$ cm^{-1}, $\hbar\omega_2 \cong 405 \pm 25$ cm^{-1}, $S_1 \cong 1.05 \pm 0.03$, $S_2 \cong 0.96 \pm 0.08$ and $\Delta\nu_{1/2} \cong 580 \pm 10$. Differences are noted between E_{00} and $\hbar\omega_1$ for the bimetallic complexes compared to their monometallic precursor. The E_{00} values are red-shifted, and their $\hbar\omega_1$ frequencies are lower. For example, for $[\{Ru(bpy)_2\}_2(Obpy)]^{4+}$, $E_{00} = 17\,370$ cm^{-1} and $\hbar\omega_1$ is 1347 cm^{-1} compared to 17 396 cm^{-1} and 1361 cm^{-1} for like parameters for $[Ru(bpy)_2(Obpy)]^{2+}$.

Discussion

Structural Considerations. While the ligands are similar, the attachment of two bipyridine moieties by way of an ethyl bridge in either the 6 or 4 position differs. The tie in the 6 position was expected to result in steric problems and thereby affect the properties and photophysics of the complexes, but such constraints were expected to be relaxed for the tie in the 4 position. Attempts were made to grow single crystals of the complexes, but these were unsuccessful. Therefore, MM2 calculations were carried out to gain insight into the possible structural constraints of the complexes.[28] The MM2 calculations for $[Ru(bpy)_3]^{2+}$ gave bond lengths of 2.05 Å and bite angles of 77° in agreement with 2.056 Å and 78° found by x-ray crystallographic[29] analysis. MM2 calculations for the complexes led to minimum energies of 61 kcal for $[Ru(bpy)_3]^{2+}$, 63 kcal for $[Ru(bpy)_2(dmb)]^{2+}$, 84 kcal for $[Ru(bpy)_2(BPY)]^{2+}$, 94 kcal for $[Ru(bpy)_2(Obpy)]^{2+}$, 116 kcal for $[Ru(bpy)(Obpy)]^{2+}$, 138 kcal for $[\{Ru(bpy)_2\}_2(BPY)]^{4+}$, and 138 kcal for $[\{Ru(bpy)_2\}_2(Obpy)]^{4+}$. In general, the increases in energy are in agreement with an increase in the complexity of the systems. The notable

(26) Caspar, J. V.; Westmoreland, T. D.; Allen, G. H.; Bradley, P. G.; Meyer, T. J.; Woodruff, W. J. *J. Am. Chem. Soc.* **1984**, *106*, 3492.
(27) Rillema, D. P.; Blanton, C. B.; Shaver, R. J.; Jackman, D. C.; Boldaji, M.; Bundy, S.; Worl, L. A.; Meyer, T. J. *Inorg. Chem.* **1992**, *31*, 1600.
(28) PCModel, Version 3.0; Serena Software: Denver, CO, 1987.
(29) (a) Rillema, D. P.; Jones, D. S.; Levy, H. *J. Chem. Soc., Chem. Commun.* **1979**, 849. (b) Rillema, D. P.; Jones, D. S.; Woods, C.; Levy, H. *Inorg. Chem.* **1992**, *31*, 2935.

exception, however, is $[Ru(bpy)(Obpy)]^{2+}$, having 50−60 kcal more energy than $[Ru(bpy)_3]^{2+}$ and $[Ru(bpy)_2(dmb)]^{2+}$. The additional energy results from steric constraints due to the dimethylene bridge located in the 6 position. The Obpy ligand in $[Ru(bpy)(Obpy)]^{2+}$ cannot assume a propeller-like arrangement as the bpy ligands do in $[Ru(bpy)_3]^{2+}$ and $[Ru(bpy)_2(dmb)]^{2+}$. MM2 calculations show that the bpy moieties of Obpy no longer are planar, having dihedral angles of 2.4 and 8.9° and bite angles of 76 and 70°, respectively. The distortion affects the Ru−N bond lengths, one to each bpy unit is increased to 2.15 Å, and the other is decreased to 2.02 Å.

The total minimized energies of the other Obpy complexes, $[Ru(bpy)_2(Obpy)]^{2+}$ and $[\{Ru(bpy)_2\}_2(Obpy)]^{4+}$, are ∼10 kcal greater than the energies of the respective BPY analogues. The structures of the BPY complexes were basically the same as $[Ru(bpy)_2(dmb)]^{2+}$, with the exception of the tethered bpy unit which assumes a configuration as distant from the attached chromophore as allowed. Distortions from the $[Ru(bpy)_2(dmb)]^{2+}$ structure were noted for $[Ru(bpy)_2(Obpy)]^{2+}$ and $[\{Ru(bpy)_2\}_2(Obpy)]^{4+}$. In $[Ru(bpy)_2(Obpy)]^{2+}$, the Ru−N bond distance neighboring the ethyl group was 2.09 Å. The other Ru−N bond distances were normal (2.05 Å). In $[\{Ru(bpy)_2\}_2(Obpy)]^{4+}$, the Ru−N bond distances neighboring the bridging ethyl group increased to 2.08 Å. Also, the Ru−Ru distance was ∼7.5 Å compared to ∼14 Å in $[\{Ru(bpy)_2\}_2(BPY)]^{4+}$.

Properties. The structural variations alter the physical properties of the complexes in subtle and sometimes unusual ways. The optical transitions pictured in Figure 2 have basically the same profiles except for $[Ru(bpy)(Obpy)]^{2+}$, which is the most distorted from D_3 or C_2 symmetry. The magnitude of the absorption coefficients for the $\pi \rightarrow \pi^*$ transitions are related to the number of diimine ligands as reported earlier.[4,6] However, the absorption coefficients for the MLCT transitions of the bimetallic complexes are not consistent with this model. For $[\{Ru(bpy)_2\}_2(BPY)]^{4+}$, it is 50% greater than for $[Ru(bpy)_2(BPY)]^{2+}$; for $[\{Ru(bpy)_2\}_2(Obpy)]^{4+}$, it is 30% greater than for $[Ru(bpy)_2(Obpy)]^{2+}$. For noninteracting metal centers, the absorption coefficient is expected to be twice as large. Three possible explanations can be given for the observed decrease. (1) The oscillator strength for optical excitation decreases upon addition of the second metal center. (2) Optical excitation of the first metal center causes a decrease in the oscillator strength for the second metal center. (3) Upon optical excitation, energy transfer occurs from one metal center to the other. The rate of energy transfer is expected to be distance dependent[30] and could account for the lower absorption coefficient enhancement of $[\{Ru(bpy)_2\}_2(Obpy)]^{4+}$ compared to $[\{Ru(bpy)_2\}_2(BPY)]^{4+}$.

As noted by redox potentials, the thermodynamic characteristics of the bimetallic complexes indicate that the metal centers are noninteracting in the ground state. The Ru^{III}/Ru^{II} redox process of both metal centers occur at, or near, the same potential. In heterocyclic ligand bridged ruthenium(II) complexes with noninsulating units separating the diimine coordinating functions, oxidation of one metal center was communicated to the second causing it to be oxidized at a more positive potential.[3] But, in the case of $[\{Ru(bpy)_2\}_2(Obpy)]^{4+}$ and $[\{Ru(bpy)_2\}_2(BPY)]^{4+}$, oxidation of the metal centers occurs at or near the same potential and, therefore, is merely a statistical mixture of the (II,II), (II,III), and (III,III) forms of the complexes.

The Obpy complexes are oxidized at a more positive potential than $[Ru(bpy)_3]^{2+}$, indicating that there is slightly more positive charge on the ruthenium centers in the Obpy compounds. This greater charge may be due to the weaker ruthenium to nitrogen bonds and/or to better overlap of the d_{xy}, d_{xz}, and d_{yz} orbitals with the π^* orbitals of the Obpy ligand. Oxidation of the BPY complexes basically follows the trend expected for CH_3 electron-donating substituents[31] which shifts the potential to less positive values. The exception to this is $[\{Ru(bpy)_2\}_2(BPY)]^{4+}$, which is oxidized approximately at the same potential as $[Ru(bpy)_3]^{2+}$. The positive shift from the Ru^{III}/Ru^{II} potential of $[\{Ru(bpy)_2\}_2(BPY)]^{4+}$ is most likely due to the greater positive charge accompanying the addition of another Ru^{II} unit to $[Ru(bpy)_2(BPY)]^{2+}$.

The first reduction occurs at nearly the same potential (-1.32 ± 0.01 V) in all of the complexes and can be assigned to reduction of one of the coordinated non-methylated bipyridine ligands. This means that the thermodynamic energy gap ($E_{ox} - E_{red}$ (1)) can be gauged by the difference in the Ru^{III}/Ru^{II} potentials. This gap has been found to correlate with emission energy maxima,[32] and, in general, the emission energy maxima (E_{00}) in this series of compounds follow this thermodynamic trend.

The temperature independent rate constant (k_0) is the sum of the nonradiative (k_{nr}) and the radiative (k_r) rate constants. Due to the fact that the complexes are weak emitters, k_{nr} can be approximated by k_0. From radiationless theory and the energy gap law,[33] the nonradiative decay rate constant is predicted to vary with S_1, the energy gap E_{00}, and $\hbar\omega_1$, as shown in eq 11. The values of k_0 in Table 5 compare favorably to the changes in E_{00}, S_1, and $\hbar\omega_1$ in Table 6. Larger values of E_{00} and smaller

$$\ln k_{nr} \propto -(S) - \gamma(E_{00}/\hbar\omega) \qquad (11)$$

where $$\gamma = (\ln E_{00}/S(\hbar\omega)) - 1$$

values of S_1 decrease k_{nr} (or k_0). These changes can be offsetting. Thus, for $[Ru(bpy)_2(BPY)]^{2+}$ and $[\{Ru(bpy)_2\}_2(BPY)]^{4+}$ which have the same k_0 values, S_1 is smaller for $[Ru(bpy)_2(BPY)]^{2+}$, $\hbar\omega_1$ is larger for $[\{Ru(bpy)_2\}_2(BPY)]^{4+}$, but E_{00} is larger for $[Ru(bpy)_2(BPY)]^{2+}$.

One of the major differences in photophysical properties is the magnitude of the emission quantum yield, ϕ_{em}, which is over 2 orders of magnitude smaller for the Obpy complexes than the others. The emission quantum yield is related to the intersystem crossing quantum yield from the ^{1}MLCT to the ^{3}MLCT state (η), the radiative rate constant (k_r) and the emission lifetime (τ_0) by the equation $\phi_{em} = \eta k_r \tau_0$. Thus, one possible reason for the decrease in ϕ_{em} can be attributed to the observed decrease in τ_0, which is reciprocal of the rate constants for various pathways of decay. The decrease in τ_0 can be attributed to steric strain imposed by the Obpy ligand in $[Ru(bpy)(Obpy)]^{2+}$ and the structural interactions in $[Ru(bpy)_2(Obpy)]^{2+}$ and $[\{Ru(bpy)_2\}_2(Obpy)]^{4+}$ resulting from attachment of the tethered unit in the 6 position of the bipyridine ring.

Other possible decreases in ϕ_{em} can be attributed to decreases in η and/or k_r. As noted before, the low-lying π^* orbitals reside on the unsubstituted bipyridine ligand. Thus, it is unlikely for k_r to change appreciably since the decay occurs from the same site in the series of complexes. A decrease in η, however, is possible given the sensitivity of the ^{3}MLCT state to solvent and temperature and to the structural problems of the Obpy series which may effectively lower the intersystem crossing probability from the value of one previously reported for $[Ru(bpy)_3]^{2+}$.[34,35]

(30) Barltrop, J. A.; Coyle, J. D. *Excited States in Organic Chemistry*; Wiley: New York, 1975; Chapter 4.

(31) (a) Hammett, L. P. *Physical Organic Chemistry*; McGraw-Hill: New York, 1940, pp 184−199. (b) Jaffe. H. H. *Chem. Rev.* **1953**, *53*, 191.

(32) Rillema, D. P.; Taghdiri, D. G.; Jones, D. S.; Keller, C. D.; Worl, L. A.; Meyer, T. J.; Levy, H. A. *Inorg. Chem.* **1987**, *26*, 578.

(33) (a) Bixon, M.; Jortner, J. *J. Chem. Phys.* **1968**, *48*, 715. (b) Freed, K. F.; Jortner, J. *J. Chem.Phys.* **1970**, *52*, 6272. (c)Engleman, R.; Jortner, J. *Mol. Phys.* **1970**, *18*, 145. (d) Freed, K. F. *Top. Curr. Chem.* **1972**, *31*, 65.

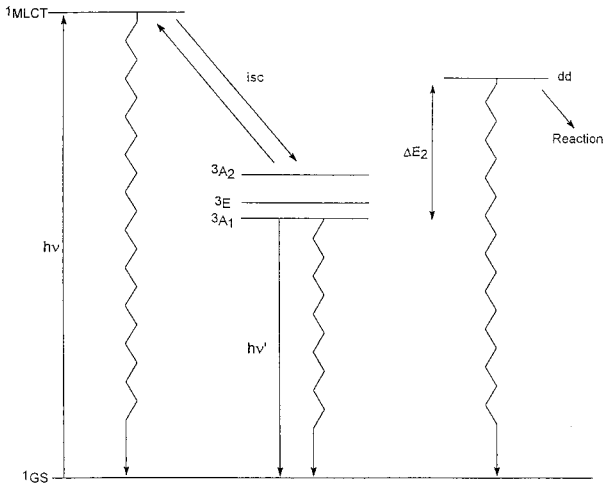

Figure 5. Energy state diagram based on the Crosby−Meyer model.

The temperature dependent emission lifetimes follow the model shown in Figure 5 originally proposed by Crosby et al.,[24,36] advanced by Meyer and co-workers,[37] Balzani and co-workers,[38] and others.[39] According to the Crosby model, the ^{3}MLCT state splits into A_1, A_2, and E levels. The energy differences between the A_1, A_2, and E states were determined by Crosby et al. in a glassy matrix in the 4−77 K range and ranged from 50 to 60 cm^{-1}. For complexes examined here, ΔE_1 varies from 100 to 241 cm^{-1} and are comparable to ΔE_1 values reported for $[Ru(bpy)_2(L-L)]^{2+}$, where L−L = 2,2′-biquinoline or one of its derivatives, which ranged from 67 to 770 cm^{-1}. In these cases the A_1, A_2, and E levels are thermally equilibrated and the ΔE_1 values are attributed to changes in the local matrix of the chromophores. The larger activation energy, ΔE_2, corresponds to populating a dd state responsible for thermal deactivation of the emitting ^{3}MLCT state at temperatures greater than 175 K for the Obpy complexes and at temperatures greater than 290 K for the BPY complexes.

The situation that is unique in the complexes compared here is the similarity of E_{00} values and the large difference in ΔE_2 values between the BPY and Obpy complexes. The lowered dd barrier in the case of the Obpy complexes can reasonably account for the decrease in emission lifetimes and emission quantum yields compared to BPY complexes by providing a more accessible deactivation channel for release of energy. This is the most likely cause of lowering the emission quantum yields and lifetimes in Obpy complexes, rather than changes in η, which was verified by the significantly larger photosubstitution quantum yield than that found for the BPY complexes. In systems reported in the past both E_{00} and ΔE_2 varied simultaneously, requiring an explanation that involved both the energy gap law and deactivation through the dd state to account for changes in emission quantrum yields and emission lifetimes. Here the π^* energy levels remain at nearly the same energy as expected for bypyridine ligands coordinated to ruthenium(II), simplifying the explanation to enhanced deactivation through the dd state for the Obpy complexes.

Acknowledgment. We thank the Office of Basic Energy Sciences of the U. S. Department of Energy and the National Science Foundation for support. We also thank Johnson-Mathey, Inc., for providing the ruthenium on loan.

IC9513447

(34) Demas, J. N.; Taylor, D. G. *Inorg. Chem.* **1979**, *18*, 3177.
(35) (a) Bensason, R.; Salet, C.; Balzani, V. *J. Phys. Chem.* **1976**, *80*, 2499. (b) Boletta, F.; Juris, A.; Mestri, M.; Sandrini, D. *Inorg. Chim. Acta* **1980**, *46*, L175.
(36) Hipps, K. W.; Crosby, G. A. *J. Am. Chem. Soc*. **1975**, *97*, 7042.
(37) (a) Meyer, T. J. *Pure Appl. Chem*. **1990**, *62*, 1003. (b) Meyer, T. J. *Pure Appl. Chem.* **1986**, *58*, 1193.
(38) (a) Barigelletti, F.; Belser, P.; von Zelewski, A.; Juris, A.; Balzani, V. *J. Phys. Chem.* **1985**, *89*, 3680. (b) Barigelletti, F.; Juris, A.; Balzani, V.; Belser, P.; von Zelewski, A. *J. Phys. Chem.* **1986**, *90*, 5190.
(39) (a)Watts, R. J. *J. Chem. Educ*. **1983**, *60*, 834, and references cited therein. (b)DeArmond, M. K. *Coord. Chem. Rev*. **1981**, *36*, 325.